Monomeric and Dimeric bZIP Transcription Factor GCN4 Bind at the Same Rate to Their Target DNA Site†

Susanne Cranz, Christine Berger, Antonio Baici, Ilian Jelesarov, and Hans Rudolf Bosshard*

Biochemisches Institut der Universität Zürich, Winterthurerstrasse 190, CH-8057 Zürich, Switzerland

Received September 3, 2003

ABSTRACT: Basic leucine zipper (bZIP) transcription factors are dimeric proteins that recognize dyadic and mostly palindromic DNA sites. Dimerization of bZIP transcription factor GCN4 is linked to the folding of its C-terminal leucine zipper domain. However, monomeric GCN4, lacking a folded leucine zipper, also recognizes the DNA site with dimerization taking place on the DNA. Here we report the kinetics of DNA recognition by unfolded monomeric and folded dimeric derivatives of GCN4 using a 19 bp double-stranded DNA containing a palindromic CRE site. The rate of DNA binding of both monomeric and dimeric GCN4 has a bimolecular rate constant of $3-5 \times 10^8$ M^{-1} s^{-1}, which is near the diffusion limit. Because the rate of dimerization of GCN4 is slower (1.7×10^7 M^{-1} s^{-1}) than the rate of DNA association, the formation of the dimeric GCN4−DNA complex through consecutive binding of two monomers (monomer pathway) is faster when starting from free monomers. Thus, the results presented here support facilitated and rapid target recognition by the monomeric transcription factor. However, DNA binding of preformed folded dimeric GCN4 is as rapid as complex formation through the monomer pathway. Therefore, the monomer and dimer pathways are kinetically equivalent if monomeric and dimeric GCN4 are at equilibrium. Hence, the dimer pathway may also have a role under *in vivo* conditions. The lower affinity of GCN4 in which two DNA contacting residues have been mutated is due exclusively to the faster dissociation of the mutant protein−DNA complex and not to slower complex formation.

Basic leucine zipper (bZIP)[1] transcription factors make up a large family of DNA binding proteins involved in the regulation of DNA transcription (*1*−*4*). These factors recognize promoter and enhancer regions of transcribed genes and, together with other protein factors, contribute to the efficiency by which RNA polymerase binds and initiates transcription. In the crystal structure of bZIP−DNA complexes, the dimeric protein binds to a DNA site with dyad symmetry, each monomer of the bZIP factor recognizing one half-site (*5*−*7*). In view of this structure, and since GCN4 and other bZIP factors dimerize in the absence of DNA, it has been thought that bZIP factors need to dimerize to recognize the DNA target site. However, the observed rapid rates of DNA binding could not be accounted for if formation of a dimeric bZIP peptide had to precede DNA binding (*8*−*11*). Thus, it has been proposed that monomeric transcription factors can recognize DNA and that these monomers dimerize while bound to DNA (*8*). This has been confirmed by experiment for several dimeric transcription factors (*10*−*15*). In the case of heterodimeric transcription factors such as Jun and Fos, initial binding of monomeric peptides could enable recognition of a different target site (for a recent review, see ref *16*). Furthermore, a monomer binding pathway may increase specificity and prevent the transcription factor from becoming trapped at nonspecific DNA sites (*10*−*12*, *14*, *15*).

Formation of a bZIP transcription factor−DNA complex via a monomer and a dimer pathway is shown schematically in Figure 1. Step 1 followed by step 2 is the dimer pathway, and step 3 followed by step 4 is the monomer pathway. The two pathways are energetically equivalent (thermodynamic cycle). However, there could be a kinetic preference for one or the other. Indeed, there is circumstantial evidence of a preferential monomer pathway even in the case of a transcription factor with a thermodynamically stable dimeric form (*15*).

For a direct comparison of the rates of formation of the peptide−DNA complex along the two pathways, one needs to separately study the kinetics of each step of Figure 1. Rapid DNA binding impedes quantitative determination of the DNA binding rates of dimeric (step 2) and monomeric (steps 3 and 4) GCN4 derivatives. As a result, we have previously only shown that an unfolded basic region peptide binds at a nearly diffusion-controlled rate (*11*). In the work presented here, we now have achieved the goal of assigning individual rate constants to steps 2 and 3 thanks to more sensitive rapid mixing instrumentation allowing for the use of lower reactant concentrations. Together with the rate constants of step 1 determined previously (*17*), we can approximate the rate constants for step 4 and predict the

† This work was supported in part by the Swiss National Science Foundation.

* To whom correspondence should be addressed: Biochemisches Institut der Universität Zürich, Winterthurerstrasse 190, CH-8057 Zürich, Switzerland. E-mail: hrboss@bioc.unizh.ch.

[1] Abbreviations: AP-1, activation protein-1 recognition site; bZIP, basic leucine zipper; CRE, cyclic AMP response element; CRE_{19}^F, double-stranded 19mer oligonucleotide containing the CRE site with the fluorescence marker NBD attached to a phosphorothioate bond preceding the recognition site; GCN4, general control of amino acid synthesis non-derepressible mutant 4 (see Table 1 for GCN4 derivatives used in this study); NBD, *N*,*N*′-dimethyl-*N*-acetyl-*N*′-(7-nitrobenzo-2-oxa-1,3-diazol-4-yl)ethylenediamine.

10.1021/bi0355793 CCC: $27.50
Published on Web 12/30/2003

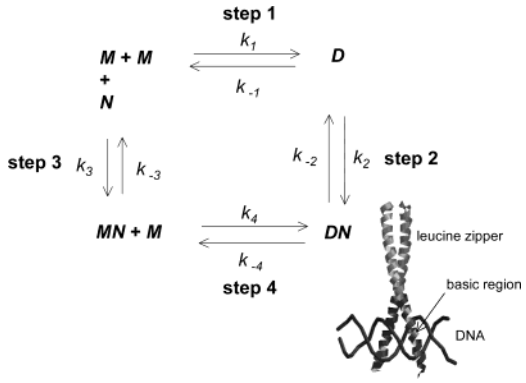

FIGURE 1: Dimer pathway (steps 1 and 2) and monomer pathway (steps 3 and 4) of association of yeast transcription factor GCN4 with its target DNA. In the dimer pathway, formation of the folded dimeric leucine zipper (step 1) precedes DNA binding of the dimer (step 2). In the monomer pathway, two monomers bind sequentially (steps 3 and 4) and the leucine zipper forms only when the second monomer binds (step 4). The reactions form a thermodynamic cycle so that $K_1K_2 = K_3K_4$ or $(k_{-1}k_{-2})/(k_1k_2) = (k_{-3}k_{-4})/(k_3k_4)$. Step 1 was studied previously (*17*). Step 2 is studied here using the derivatives C62GCN4, C62GCN4$_{SS}$, C62GCN4$_{AK}$, and BR$_{SS}$ and step 3 using derivatives C62GCN4$_{SS}^{one-leg}$ and BR (see Table 1 for structures of GCN4 derivatives). The three-dimensional structure of the GCN4−DNA complex (bottom right) is adapted from ref *7*.

overall rates of DNA binding via the monomer and dimer pathway, respectively. The results demonstrate that in the isolated system studied here, which is composed of a 19mer double-stranded DNA target and the 62-residue C-terminal DNA-binding domain of GCN4, both the monomeric and the dimeric transcription factor recognize the palindromic CRE target site at the same rapid rate. Since the rate of formation of the dimer in step 1 is significantly slower than the rates of DNA binding in steps 2−4, the monomer pathway is more rapid than the dimer pathway when starting from two monomeric GCN4 proteins and no dimer, but not when monomeric and dimeric GCN4 are at equilibrium.

EXPERIMENTAL PROCEDURES

Materials

The plasmid pET-3AC62GCN4 was used to express the 62-residue C-terminal fragment (residues 220−281) of GCN4 in *Escherichia coli* (*18*) to obtain C62GCN4 and C62GCN4$_{SS}$ as described previously (*19*). GCN4 variants BR, BR$_{SS}$, and LZ (see Table 1 for sequences) were chemically synthesized by employing the Fmoc strategy (*20*). The variant C62GCN4$_{SS}^{one-leg}$, termed "one-legged", was produced by subjecting equal amounts of reduced C62GCN4$_{SS}$ and LZ to air oxidation and purifying the products by reverse phase HPLC. Mutant C62GCN4$_{AK}$ was obtained by PCR mutagenesis according to a modified protocol (*21*). The mutations were introduced in two consecutive steps using the following templates: 5′-CAA CTT TCT CGC TTT AGA ACG CCT GCG-3′ for R243K, 5′-GGC GGC TTC AGT GGC TCT AGC ACG TTT-3′ for N235A, and 5′-ATA ATG GCC TGC TTC TCG CCG AAA CG-3′ as the back primer for both mutations. Changes with respect to the wild-type sequence are underlined.

The identity and purity of all peptides were determined by ion spray mass spectrometry. Peptide concentrations were calculated from the absorption at 280 nm using the following absorption coefficients (*22*): $\epsilon = 1280$ cm^{-1} M^{-1} for C62GCN4 and C62GCN4$_{AK}$, $\epsilon = 1340$ cm^{-1} M^{-1} for C62GCN4$_{SS}$, BR$_{SS}$, and C62GCN4$_{SS}^{one-leg}$, and $\epsilon = 1400$ cm^{-1} M^{-1} for BR. All concentrations refer to a single peptide chain, unless indicated otherwise.

The oligonucleotide TGG*t*AGATGACGTCATCTCC containing a phosphorothioate group between the third and fourth bases was obtained from MicroSynth (Balgach, Switzerland). It was labeled with the fluorescent group NBD (Molecular Probes, Eugene, OR) to obtain the fluorescent oligonucleotide CRE$_{19}^{F}$. The identity and purity of the product were confirmed by ion spray mass spectrometry. CRE$_{19}^{F}$ or CRE$_{19}$ (oligonucleotide without the fluorescent group) was annealed by heating to 90 °C and slow cooling to room temperature. The concentration of single-stranded DNA was calculated from the absorption at 260 nm using an ϵ of 198.1 mM^{-1} cm^{-1} for CRE$_{19}^{F}$ and an ϵ of 180.5 mM^{-1} cm^{-1} for CRE$_{19}$ (*23*). Given concentrations always refer to double-stranded DNA.

Methods

Buffer. All experiments were conducted at 6.5 °C in 50 mM Tris-HCl, 10 mM NaCl, and 10 mM $MgCl_2$ (pH 7.8, ionic strength of 68 mM).

Kinetic Experiments. Rates of peptide−DNA association were studied with an SX.18MV-R stopped-flow spectrometer from Applied Photophysics (Surrey, U.K.). Equal volumes of reagent solutions were mixed (dead time of <3 ms), and the change in fluorescence emission above 515 nm was measured after excitation at 495 nm. Six or more firings were averaged for each kinetic trace. In one series of experiments, equally or similarly concentrated solutions of CRE$_{19}^{F}$ and peptide were mixed. In another series, the peptide was present in excess over CRE$_{19}^{F}$, the concentration of which was kept constant at 20 nM.

To follow the dissociation of the peptide−DNA complexes, 50−100 nM CRE$_{19}^{F}$ and 50−100 nM peptide (monomer or dimer) were pre-equilibrated to form the peptide−DNA complex. The pre-equilibrated complex was mixed with nonfluorescent CRE$_{19}$ in a 40-fold excess over CRE$_{19}^{F}$. The fluorescence decrease caused by the exchange of CRE$_{19}$ for CRE$_{19}^{F}$ was followed with the fluorescence emission above 515 nm (excitation at 495 nm). When the dissociation reaction was slow, mixing was performed manually and the fluorescence decrease at 544 nm (excitation at 495 nm) was followed with a Spex Fluorolog instrument. In manual mixing (mixing time of 5−10 s), 50 μL of CRE$_{19}$ was added to 1.8 mL of a stirred solution of the preformed peptide−CRE$_{19}^{F}$ complex. We did not correct for the small dilution of the preformed complex on addition of CRE$_{19}$.

Equilibrium Fluorescence Titration and Isothermal Titration Calorimetry. Fluorescent titrations were performed in a Perkin-Elmer LS50 luminescence spectrometer by stepwise addition of small volumes of a 5−200 μM peptide solution to 1.8 mL of 125 nM CRE$_{19}^{F}$ placed in the cuvette, and the fluorescence emission in the range of 510−600 nm (excitation at 495 nm) was integrated. Peptide BR was titrated to the nonfluorescent labeled AP-1 site in a titration calorimeter (MCS ITC, MicroCal Inc., Northampton, MA) as described previously (*19*). Calorimetric titrations were performed at 6.5 °C in 50 mM sodium phosphate buffer and 100 mM NaCl (pH 7).

Table 1: Derivatives of Yeast Transcription Factor GCN4 and the Fluorescent Target DNA Site Used in This Study[a]

	Basic region leucine zipper
C62GCN4 [b]	MIVPESSDPAAL*KRARNTEAARRSRARK*LQRMKQ-LEDKVEELLSKNYHLENEVARLKKLVGER
$C62GCN4_{SS}$	MIVPESSDPAALKRARNTEAARRSRARKLQRMKQ-LEDKVEELLSKNYHLENEVARLKKLVGERGSGC | MIVPESSDPAALKRARNTEAARRSRARKLQRMKQ-LEDKVEELLSKNYHLENEVARLKKLVGERGSGC
$C62GCN4_{AK}$ [c]	MIVPESSDPAALKRARATEAARRSKARKLQRMKQ-LEDKVEELLSKNYHLENEVARLKKLVGER
$C62GCN4_{SS}^{one-leg}$	MIVPESSDPAALKRARNTEAARRSRARKLQRMKQ-LEDKVEELLSKNYHLENEVARLKKLVGERGSGC | Ac-RMKQ-LEDKVEELLSKNYHLENEVARLKKLVGERGSGCG-NH_2
LZ	Ac-RMKQ-LEDKVEELLSKNYHLENEVARLKKLVGERGSGCG-NH_2
BR	Ac-YPESSDPAALKRARNTEAARRSRARKLQRMKQGGC(StBu)G-NH_2
BR_{SS}	Ac-YPESSDPAALKRARNTEAARRSRARKLQRMKQGGCG-NH_2 | Ac-YPESSDPAALKRARNTEAARRSRARKLQRMKQGGCG-NH_2
CRE_{19}^{F} [d]	5′-TGG^{NBD}AGATGACGTCATCT···CC-3′ 3′-CC···TCTACTGCAGTAGA^{NBD}GGT-5′

[a] Sequence differences with respect to the wild-type GCN4 sequence are underlined. Ac, N^{α}-acetyl; NH_2, amide; StBu, thio-*tert*-butyl. [b] This sequence corresponds to C-terminal residues 220−281 of GCN4 and the N-terminal Met from the expression construct (*18*). Residues of the basic region contacting the DNA are italicized. [c] Basic region N235A and R243K mutations (*32*) are underlined. [d] CRE site with the NBD fluorescence tag, with the palindromic recognition sequence underlined.

Data Analysis. A sum of exponentials was used to fit the kinetic traces according to

$$F(t) = F_0 + \sum_i a_i[1 - \exp(-k_i^{app}t)] \quad (1)$$

where k_i^{app} values are apparent rate constants, a_i values are amplitudes, and F_0 is the fluorescence signal at time zero. Kinetic traces for monomer binding (step 3 of Figure 1) were best fit by a single-exponential fluorescence increase, and rate constants were obtained from (*24*)

$$k_3^{app} = k_3([M_{eq}] + [N_{eq}]) + k_{-3} \quad (2)$$

where $[M_{eq}] + [N_{eq}]$, the sum of the concentrations of the peptide monomer and single-stranded DNA at equilibrium, was estimated using the K_3 determined by fluorescence titration. When the total peptide concentration was much larger than the total DNA concentration, $[M_{eq}] + [N_{eq}]$ was approximated by $[M_{tot}]$. Alternatively, k_3 and k_{-3} of single-exponential kinetic traces were obtained by solving eq 3:

$$\frac{d[MN]}{dt} = k_3([N_0] - [N])([M_0] - [M]) - k_{-3}[MN] \quad (3)$$

where $[M_0]$ and $[N_0]$ refer to the initial peptide and DNA concentration, respectively. At any time point of the reaction

$$[MN(t)] = [N_0] - [N(t)] \quad (4)$$

where $[MN(t)]$ is the integral of eq 3. The decrease of free DNA with time, $[N(t)]$, is related to the fluorescence increase described by the kinetic trace according to

$$\frac{[N(t)]}{[N_0]} = \frac{F_\infty - F(t)}{F_\infty - F_0} \quad (5)$$

where $F(t)$ is the fluorescence signal at time t and F_0 and F_∞ are the fluorescence signals at time zero and infinite time, respectively. Combining eqs 4 and 5 gives

$$F(t) = F_\infty - \frac{(F_\infty - F_0)([N_0] - [MN(t)])}{[N_0]} \quad (6)$$

To obtain k_3, k_{-3}, F_0, and F_∞, kinetic traces of step 3 were analyzed by nonlinear fitting with the help of eq 6 using the integral of eq 3 to calculate $[MN(t)]$. Since simultaneous determination of all four parameters tended to produce poor estimates of k_3 and k_{-3} because of ill-defined arrays during the fitting procedure, F_∞ was estimated from the experimental trace and kept constant during the nonlinear fitting procedure, which was performed with the program SigmaPlot (version 7.0).

The best fit for dimer binding (step 2 of Figure 1) was obtained by a two-exponential fluorescence increase. The rate constants were obtained from (*24*)

$$k_2^{app} = k_2([D_{eq}] + [N_{eq}]) + k_{-2} \quad (7a)$$

$$k'^{app}_2 = k'_2\frac{k_2([D_{eq}] + [N_{eq}])}{k_2([D_{eq}] + [N_{eq}]) + k_{-2}} + k'_{-2} \quad (7b)$$

The above equations describe a biphasic reaction between two reactants in which the rapid phase exhibits a linear concentration dependence and the slow phase a hyperbolic dependence (*24*). k_2^{app} is the apparent rate constant of the first rapid phase of the experimental trace and k'^{app}_2 that of the slow phase. $[D_{eq}] + [N_{eq}]$ was estimated with the help of K_2 from fluorescence titration. Under the given experimental conditions, $k_2([D_{eq}] + [N_{eq}])$ was much larger than k_{-2}, so eq 7b can be reduced to $k'^{app}_2 \cong k'_2 + k'_{-2}$.

Dissociation constants, K, were obtained from fluorescence titration data by fitting the integrated fluorescence signal, F, according to

$$F = [(F_\infty - F_0)([N_0] + [P_0] + K - \sqrt{([N_0] + [P_0] + K)^2 - 4[N_0][P_0]}]/(2[N_0] + F_0) \quad (8)$$

where F_0 and F_∞ are the initial and final fluorescence signal, respectively. In the case of the monomeric derivatives BR and C62GCN4$_{SS}^{one-leg}$, $[P_0]$ is the total concentration of a single DNA binding site and $[N_0]$ the total concentration of one half-site of double-stranded CRE$_{19}^{F}$. In the case of dimeric derivatives C62GCN4, C62GCN4$_{SS}$, C62GCN4$_{AK}$, and BR$_{SS}$, $[P_0]$ is the total concentration of the dimeric peptide and $[N_0]$ the total concentration of double-stranded CRE$_{19}^{F}$.

Error Estimates. Standard errors of the regression of the fits to the experimental data are shown unless indicated.

RESULTS

Design of Monomeric and Dimeric Derivatives of GCN4 for Analyzing Single Steps of the Monomer and Dimer Pathway. Transcriptional activator GCN4 is a homodimeric protein composed of two polypeptide chains of 281 residues each (*25*, *26*). The 30 C-terminal residues contain four heptadic repeats that induce dimerization by formation of a leucine zipper (*5*, *27*). Upon DNA binding, the α-helices of the leucine zipper extend N-terminally into a long bipartite structure that grips the large groove of double-stranded DNA (*1*). The structure is shown in outline at the bottom right of Figure 1. The C-terminal 60-residue segment of GCN4 is sufficient for DNA recognition (*28*). It is composed of a basic region responsible for specific DNA recognition, followed by the C-terminal leucine zipper (Table 1). The basic region recognizes the target sequences ATGACTCAT named the AP-1 site and ATGACGTCAT named the CRE site (*29*). The latter differs from the AP-1 site by an additional G (underlined), which makes the CRE site palindromic. Both target sites are recognized with the same overall affinity (*19*, *30*). The 62 C-terminal residues of GCN4 (residues 220−281), called C62GCN4 (*19*), together with a 19 bp DNA comprising the CRE site were used in this study. DNA association was monitored with the help of the fluorescently labeled oligonucleotide CRE$_{19}^{F}$ (Table 1). The level of fluorescence emission of the NBD group of CRE$_{19}^{F}$ increases on binding to the basic region of GCN4, the fluorescence change being specific for the AP-1 and CRE sites (*11*). CRE$_{19}^{F}$ harboring the CRE site was used here because it exhibits a somewhat larger fluorescence change upon binding than the NBD-labeled AP-1 site (*11*).

The combined monomer and dimer pathways are described by a minimum of four equilibrium and eight rate constants (Figure 1). In principle, all the rate constants may be obtained by simultaneous fitting of kinetic traces acquired by mixing the peptide and DNA at a series of different concentrations using a numerical fitting algorithm (*31*). In practice, however, experimental noise prevents the unequivocal assignment of rate constants to each step (*15*). As an alternative, we decided to study single steps of Figure 1 with the help of appropriate monomeric and dimeric derivatives of GCN4 (Table 1).

Thermodynamics and kinetics of reaction step 1 (leucine zipper formation in the absence of DNA) have been analyzed previously (*17*). Association of dimeric GCN4 with DNA in reaction step 2 was studied in four different ways: (i) with the disulfide-linked, permanently dimeric derivative C62GCN4$_{SS}$, (ii) with C62GCN4 sufficiently concentrated to make the monomer concentration negligible, (iii) with disulfide-linked basic region peptide BR$_{SS}$ lacking the leucine zipper domain, and (iv) with sufficiently concentrated mutant derivative C62GCN4$_{AK}$ in which two conserved residues contacting the DNA are mutated to weaken DNA binding without destabilizing the leucine zipper dimer (*32*). Reaction step 3, which is DNA association of the monomer, was investigated with two derivatives: the basic region peptide BR and the one-legged derivative C62GCN4$_{SS}^{one-leg}$. The latter is the disulfide-linked dimeric leucine zipper with only a single basic DNA-binding region. Finally, estimates of equilibrium and rate constants for the binding of the second monomer in step 4 were obtained from the thermodynamic cycle described in Figure 1.

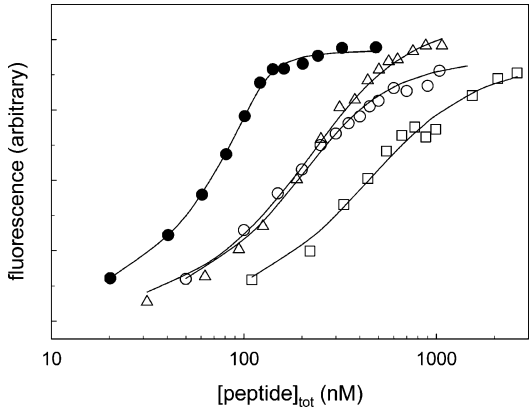

FIGURE 2: Titration of 125 nM double-stranded CRE$_{19}^{F}$ with C62GCN4 (●), C62GCN4$_{AK}$ (△), C62GCN4$_{SS}^{one-leg}$ (○), and BR (□). Solid lines are best fits according to eq 8 describing a 1/1 complex.

Equilibrium Fluorescence Titration. Dissociation constants of the peptide−DNA complexes were calculated from the fluorescence increase observed when CRE$_{19}^{F}$ was titrated with the monomeric or dimeric peptide. Representative titrations are shown in Figure 2, and constants K_2 and K_3 are given in Tables 2 and 3, respectively. As expected, the best binders are the dimeric wild-type peptides C62GCN4 and C62GCN4$_{SS}$. Their K_2 values (Table 2) are around 2 nM, the error of K_2 being large since fluorescence titrations had to be performed at peptide and DNA concentrations that were much higher than K_2. Independent isothermal titration calorimetry of CRE$_{19}$ with C62GCN4 at 9 °C, pH 7.6, and an ionic strength of 190 mM yields a K_2 of 6.3 ± 3.3 nM (*19*). The dimeric derivative C62GCN4$_{AK}$ in which two residues contacting DNA have been mutated shows weaker binding with a K_2 of 114 ± 48 nm.

It should be noted that K_2 refers to a 1:1 complex of the dimeric peptide and double-stranded CRE$_{19}^{F}$; i.e., the binding of the two legs of the dimeric peptide to the two half-sites of CRE is regarded as a single binding event. This simplification is justified under equilibrium conditions since the dimeric peptides were either disulfide-linked (C62GCN4$_{SS}$ and BR$_{SS}$) or present at a sufficiently high concentration to make the monomer concentration negligible (C62GCN4 and C62GCN4$_{AK}$).

The value of K_3 for monomer binding was attained using monomeric BR and C62GCN4$_{SS}^{one-leg}$ as GCN4 derivatives which make contact with only one half-site. Monomeric BR is the most weakly binding derivative with a K_3 of ~400

Table 2: Kinetic Rate Constants and Equilibrium Dissociation Constants for DNA Binding of Dimeric GCN4 Derivatives (Step 2 of Figure 1)

	$D+N \underset{k_{-2}}{\overset{k_2}{\rightleftarrows}} DN^* \underset{k'_{-2}}{\overset{k'_2}{\rightleftarrows}} DN$			DNA displacement [c]	$K_2 = \frac{[D][N]}{[DN^*]+[DN]}$ [d]
	k_2 ($M^{-1}s^{-1}$) [a]	k_{-2} (s^{-1}) [a]	$k'_2 + k'_{-2}$ (s^{-1}) [b]	k_{disp} (s^{-1})	(nM)
C62GCN4	$(3.0 \pm 1.3) \times 10^8$	36 ± 15	10 ± 8	$(2.4 \pm 0.8) \times 10^{-4}$	≈ 2
$C62GCN4_{SS}$	$(3.4 \pm 1.4) \times 10^8$	25 ± 20	10 ± 8	$(5.4 \pm 1.6) \times 10^{-4}$	1.5 ± 1.0 [e]
$C62GCN4_{AK}$	$(7.7 \pm 2.5) \times 10^8$	[f]	1.1 ± 0.2	5.0 ± 0.2	114 ± 48
BR_{SS}	$(7.0 \pm 2.5) \times 10^8$	[f]	8 ± 5	≈ 0.02 [g]	58 ± 22

[a] From plot according to eq 7a. [b] From plot according to eq 7b and the limiting case of $k_2([D_{eq}] + [N_{eq}]) \gg k_{-1}$. [c] Dilution of the complex with an excess of nonfluorescent CRE_{19}. [d] Fluorescence titration of CRE_{19}^F with peptide. [e] From ref *11*. [f] Could not be determined because of the large error. [g] The displacement reaction shows two exponential phases; the overall $t_{1/2}$ is 3.5 s.

Table 3: Kinetic Rate Constants and Equilibrium Dissociation Constants for DNA Binding of Monomeric GCN4 Derivatives (Step 3 of Figure 1)

	$M+N \underset{k_{-3}}{\overset{k_3}{\rightleftarrows}} MN$		$K_3 = \frac{k_{-3}}{k_3}$	DNA displacement [c]	$K_3 = \frac{[M][N]}{[MN]}$ [d]
	k_3 ($M^{-1}s^{-1}$)	k_{-3} (s^{-1})	*(nM)*	k_{disp} (s^{-1})	(nM)
$C62GCN4_{SS}^{one-leg}$	$(4.6 \pm 1.2) \times 10^8$ [a]	66 ± 18 [a]	140 ± 54	6.2 ± 0.2	121 ± 11
	$(6.4 \pm 4.3) \times 10^8$ [b]	33 ± 16 [b]	52 ± 42		
BR	$(5.1 \pm 1.5) \times 10^8$ [b]	83 ± 20 [b]	163 ± 62	73 ± 5	406 ± 32

[a] From plot according to eq 2. [b] From data analysis according to eq 6. [c] Dilution of the complex with an excess of nonfluorescent CRE_{19}. [d] From fluorescence titration of CRE_{19}^F with peptide.

nM. $C62GCN4_{SS}^{one-leg}$ has a K_3 of 121 ± 11 nM, similar to the K_2 measured for the dimeric derivative $C62GNC4_{AK}$ in which two residues contacting DNA have been mutated and similar to the K_2 of the "minimal" dimer BR_{SS} composed of two disulfide-linked basic region peptides.

DNA Association of Dimeric Derivatives of GCN4. Kinetic traces for GCN4 derivatives with two DNA binding sites exhibit two exponential phases: an initial rapid phase, which depends linearly on peptide concentration, and a slow and apparently concentration-independent phase. This behavior can be explained by the following mechanism:

$$D + N \underset{k_{-2}}{\overset{k_2}{\rightleftharpoons}} DN^* \underset{k'_{-2}}{\overset{k'_2}{\rightleftharpoons}} DN$$

where D is the dimeric peptide, N is CRE_{19}^F, DN* is an intermediate, and DN is the final complex. The four rate constants are related to the two apparent rate constants k_2^{app} and k'^{app}_2 as described by eqs 7a and 7b in Methods. The amplitude of the slower phase described by k'^{app}_2 decreases at increasing peptide concentrations so that k'^{app}_2 could no longer be measured above ~200 nM peptide. A small amount of monomeric C62GCN4 or $C62GCN4_{AK}$ at equilibrium with the corresponding dimer could be neglected since K_1 of the monomer−dimer equilibrium (step 1 of Figure 1) is 6 nM at 5 °C (*17*), similar to the *K* of 8 nM reported for the leucine zipper domain alone (*33*). Therefore, C62GCN4 was 85% dimeric already at the lowest peptide concentration used in kinetic experiments. Figure 3A shows a kinetic trace for the reaction of C62GCN4 with CRE_{19}^F. Plots of the observed rate constants k_2^{app} and k'^{app}_2 versus the equilibrium concentrations ($[D_{eq}] + [N_{eq}]$) are shown in Figure 3B. While k_2 could be calculated with good accuracy, k_{-2} extrapolated from *y*-intercepts had a very large error. In principle, k'_2 and k'_{-2} of the slow phase can be obtained from plots according to eq 7b provided the experiment can be performed at a sufficiently low reactant concentration. This was not possible, and experimental errors were large because of the small amplitude of the second phase. Therefore, only a rough estimate of $(k'_2 + k'_{-2})$ could be obtained. Rate constants for the dimeric derivatives are summarized in Table 2.

DNA Association of Monomeric Derivatives of GCN4. Figure 4A shows a representative trace of the reaction of $C62GCN4_{SS}^{one-leg}$ with CRE_{19}^F. Binding of one-legged GCN4 and binding of the monomeric DNA binding domain BR exhibit a single-exponential phase described by

$$M + N \underset{k_3}{\overset{k-3}{\rightleftharpoons}} MN$$

Here, M corresponds to the single DNA-binding site of $C62GCN4_{SS}^{one-leg}$ or to a single basic region peptide BR, and *N* is a half-site of double-stranded CRE_{19}^F. Rate constants k_3 and k_{-3} were obtained by plotting apparent rate constants according to eq 2. The plot for $C62GCN4_{SS}^{one-leg}$ is shown in Figure 4B. Alternatively, kinetic traces were also fit according to eq 6, which is based on the integrated rate equation, eq 3 (solid line in Figure 4A). The bimolecular association rates of $C62GCN4_{SS}^{one-leg}$ and BR are $\sim 5 \times 10^8$ M^{-1} s^{-1}, indistinguishable within experimental error (Table 3). Also, the dissociation rate constants k_{-3} of the MN complexes are similar but have a large error from extrapolation to the *y*-axis intercept, as has k_{-3} from fitting with eq 6.

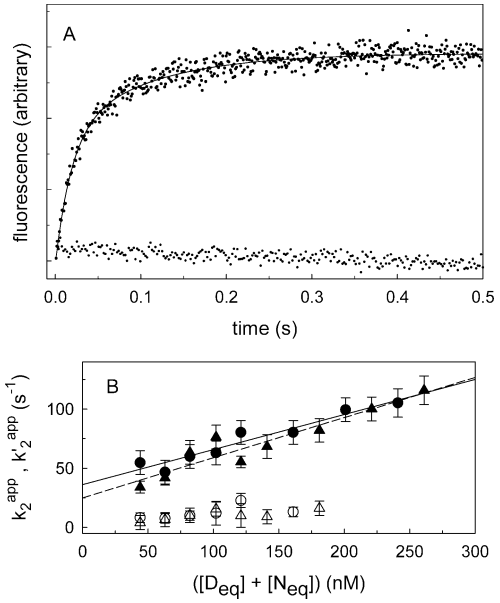

FIGURE 3: Representative kinetic trace of the association of dimeric C62GCN4 with DNA. (A) Reaction of 140 nM dimeric C62GCN4 with 20 nM CRE_{19}^{F}. The solid line is a best fit for a k_2^{app} of 53 s^{-1} (amplitude of 73%) and a k'^{app}_2 of 9 s^{-1} (amplitude of 27%). The bottom trace shows the control reaction of CRE_{19}^{F} with the basic peptide EYQALKKKVAQLKAKNQALKKKVAQLKHKG, whose sequence is unrelated to the basic region of C62GCN4 (see ref *11* for details). (B) Apparent rate constants k_2^{app} (filled symbols) and k'^{app}_2 (empty symbols) for DNA binding of C62GCN4 (circles, solid line) and $C62GCN4_{SS}$ (triangles, dashed line) plotted according to eq 7a and 7b, respectively. Error bars indicate the data range of two or three independent experiments.

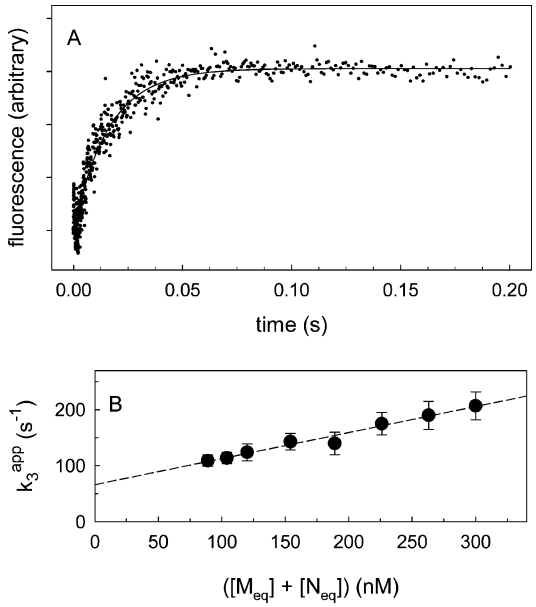

FIGURE 4: Representative kinetic trace of association of monomeric GCN4 with DNA. (A) Reaction of 35 nM one-legged derivative $C62GCN4_{SS}^{one-leg}$ with 35 nM CRE_{19}^{F}. The solid line is a best fit according to eq 6. (B) Apparent rate constant k_3^{app} for DNA binding of $C62GCN4_{SS}^{one-leg}$ plotted according to eq 2. Error bars indicate the data range of two or three independent experiments.

The dissociation constant K_3 calculated as k_{-3}/k_3 is in the range of 50−140 nM for $C62GCN4_{SS}^{one-leg}$, in agreement with K_3 from fluorescence titration. For the monomer BR, K_3 from kinetics is 3 times smaller than from fluorescence titration.

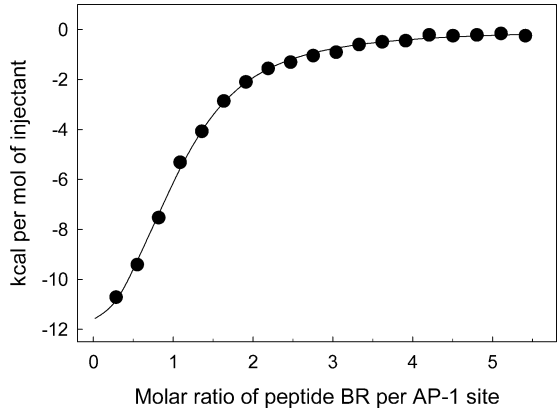

FIGURE 5: Calorimetric titration of the AP-1 site with basic region peptide BR. The solid line is a best fit for a stoichiometry n of 0.96 and a K_3 of 2 μM, which is larger than the K_3 obtained by fluorescence titration (Table 3), probably because of the higher ionic strength applied in calorimetry.

The measured rate constants and dissociation constants might not pertain to step 3 alone but could encompass steps 3 and 4 together if two monomeric peptides bind to the dyadic CRE site. This is very unlikely for $C62GCN4_{SS}^{one-leg}$ since the two coiled coils from two molecules of $C62GCN4_{SS}^{one-leg}$ would interfere with each other in the orientation seen in the crystal structure of the wild-type complex (Figure 1). Less steric hindrance is expected for the binding of two molecules of BR. Isothermal titration calorimetry showed, however, that only a single BR binds to the two half-sites (Figure 5). The stoichiometry is 0.96 mol of BR per mole of double-stranded DNA. Furthermore, the heat capacity change for binding of a single BR molecule is roughly half that for binding of dimeric C62GCN4 (I. Jelesarov and C. Berger, unpublished experiments). Hence, the kinetic and equilibrium data obtained with the monomeric derivative BR pertain to step 3 alone.

Dissociation Rates Estimated from DNA Displacement. An independent estimate of the overall dissociation rate constant of the peptide−DNA complexes was obtained from dilution of the preformed peptide−CRE_{19}^{F} complex with an excess of nonfluorescent DNA according to

$$P{-}CRE_{19}^{F} + CRE_{19} \xrightarrow{k_{disp}} P{-}CRE_{19} + CRE_{19}^{F} \quad (9)$$

where P is either monomer M or dimer D. In the case of a complex in which only one half-site of the DNA is contacted by the peptide, the observed rate constant of DNA displacement, k_{disp}, should be equivalent to k_{-3} if the rate of rebinding of nonfluorescent CRE_{19} is much faster than the dissociation of the complex. Rebinding, calculated as k_3[CRE_{19}], was ca. 1000 s^{-1} under the chosen experimental conditions, much faster than k_{-3}. Figure 6A shows DNA displacement from the $C62GCN4_{SS}^{one-leg}$−CRE_{19}^{F} complex. The reaction obeys a single-exponential decay with a k_{disp} of 6.2 s^{-1}, a value 5−10 times slower than k_{-3} obtained from binding traces (Table 3). In the case of the BR−CRE_{19}^{F} complex, DNA displacement has a rate of 73 ± 5 s^{-1}, in good agreement with k_{-3} from binding traces (Table 3).

DNA displacement from dimeric C62GCN4 and $C62GCN4_{SS}$ is very much slower and has a half-time of ∼40 min (Figure 6B). Even DNA displacement from the complex with

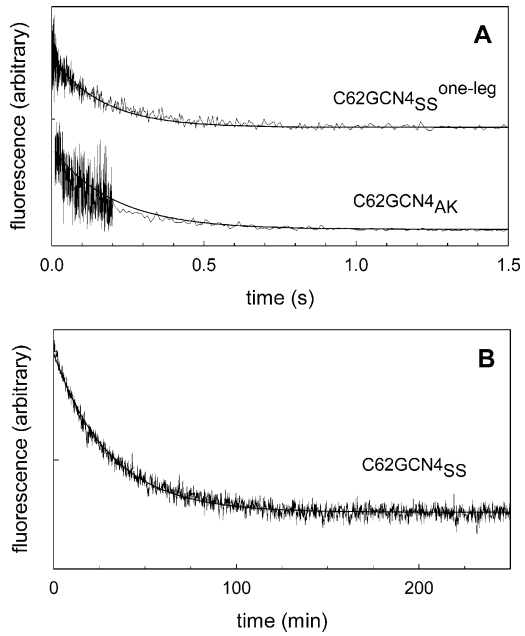

FIGURE 6: Displacement of DNA from the preformed protein−DNA complex. (A) Approximately 20 nM preformed complex composed of CRE_{19}^{F} and $C62GCN4_{SS}^{one-leg}$ or $C62GCN4_{AK}$ was diluted with 2 μM nonfluorescent CRE_{19}. The solid lines are best fits for k_{disp} values of 6.2 s^{-1} ($C62GCN4_{SS}^{one-leg}$) and 5 s^{-1} ($C62GCN4_{AK}$) based on the data from six independent experiments. The traces are shifted with respect to the *y*-axis for clarity. (B) Approximately 40 nM preformed complex composed of $C62GCN4_{SS}$ and CRE_{19}^{F} was diluted with 2 μM nonfluorescent CRE_{19}. The solid line is a best fit for a k_{disp} of 2.4×10^{-4} s^{-1}. Note the different scale of the time axes in panels A and B.

the "minimal" dimer BR_{SS} has a halftime of ~1 min, significantly slower than the dissociation of the one-legged complex. However, DNA displacement from the dimeric mutant $C62GNC4_{AK}$, which binds DNA more weakly than wild-type C62GCN4, is roughly as fast as DNA displacement from the monomeric one-legged peptide (Figure 6A).

DISCUSSION

Understanding the forces involved in protein−DNA recognition requires careful and systematic analysis of the thermodynamics and kinetics of protein−DNA association. Electrophoretic mobility shift assays are often used to investigate protein−DNA interactions. However, this assay may be problematic because it is not at equilibrium and complexes may dissociate during electrophoresis. Monomer−DNA complexes in particular might escape detection because they are kinetically unstable. Environmentally responsive fluorescence probes allow us to follow protein−DNA association reactions by rapid mixing in the second to millisecond time range. Patel and co-workers (*34*) and Kohler and Schepartz (*15*) attached different fluorescence tags to the leucine zipper part of Jun and Fos to monitor resonance energy transfer when the Jun−Fos heterodimer forms in the presence and absence of DNA, respectively. Via this elegant approach, it was shown that dimerization of Jun and Fos is more rapid in the presence of DNA (*15*, *34*), that the Jun−Fos−DNA complex is extremely stable (*34*), and that its formation follows the monomer pathway (*15*).

Since our goal was the direct comparison of the monomer and dimer pathway of DNA binding, following the reaction by visualizing dimer formation from a fluorescence tag in the leucine zipper domain was not applicable. The fluorescence tag was attached on the DNA instead. An NBD group was placed next to the palindromic CRE site to obtain CRE_{19}^{F}. Fluorescence emission of NBD reports sequence specific binding to the CRE and AP-1 sites but not unspecific, electrostatically driven DNA binding (control trace in Figure 3 and ref *11*). One disadvantage of attaching the fluorescence tag to the DNA is that experiments are restricted to short oligonucleotides since the fluorescence signal becomes very weak when long pieces of double-stranded DNA are used as these cannot be sufficiently concentrated for the kind of rapid mixing experiments performed here. In contrast, peptide binding to a heterogeneous mixture of large DNA fragments from calf thymus could be monitored when the fluorescence tag was attached to the leucine zipper domain (*15*)

Dimer Pathway. Formation of dimeric C62GCN4 in the absence of DNA (step 1 of Figure 1) has been studied in detail previously (*17*). At 5 °C, the dissociation constant of dimeric C62GCN4 is 6 nM; the rate constants of dimer formation and dissociation are 1.6×10^{7} M^{-1} s^{-1} and 0.1 s^{-1}, respectively.

Binding of dimeric derivatives of GCN4 to the CRE site in a 19mer oligonucleotide exhibits two kinetic phases: a rapid, concentration-dependent phase and a slow, apparently concentration-independent phase. The reaction is interpreted as the concentration-dependent formation of an initial complex DN*, which rearranges in a concentration-independent step to the thermodynamically stable complex DN. The nature of the intermediate DN* and its rearrangement to DN are unknown. One is tempted to speculate that DN* is an intermediate with only "one leg" bound to one DNA half-site and that the rearrangement conforms to the intramolecular binding of the "second leg" to the second half-site. In support of this proposition, binding of mutant $C62GCN4_{AK}$, whose binding strength is similar to that of the monomeric derivatives, also exhibits two exponential reaction phases, whereas monomer binding is always single-exponential.

The association rate constant k_2 for the D + N → DN* reaction is 3×10^{8} M^{-1} s^{-1}, which is not far from a diffusion limit of 5×10^{9} M^{-1} s^{-1} estimated by the von Smolukowski relationship for the association of uncharged molecules (*35*, *36*). The diffusion limit could be larger because of electrostatic attraction between the charged reactants. Similar rates have been reported for the binding of the *E. coli* SSB protein to single-stranded DNA (*37*) and for DNA binding of the papilloma E2 protein (*38*).

The two reaction phases of dimer binding are coupled so that the DN* → DN rearrangement should exhibit hyperbolic concentration dependence (eq 7b). This was not seen because reactant concentrations had to be relatively large and the scatter of $k_2'^{app}$ was considerable. Since the amount of intermediate DN* will be small at equilibrium, k_2' has to be significantly larger than k_{-2}', which means $k_{-2}' \ll k_2'^{app}$. If we assume the equilibrium is 100 times on the side of the final complex DN, k_2' would be similar to $k_2'^{app}$ (≈10 s^{-1}) and k_{-2}' would be ~0.1 s^{-1}. Using these values of k_2' and k_{-2}' together with a k_2 of 3×10^{8} M^{-1} s^{-1} and a k_{-2} of 30 s^{-1}, the overall equilibrium constant K_2 for DNA binding to

dimeric C62GCN4 and C62GCN4$_{SS}$ is 1 nM,[2] in agreement with the K_2 estimated by fluorescence titration. The overall dissociation constant of the dimer pathway is K_1K_2 and amounts to 6×10^{-18} M^2 for C62GCN4, in good agreement with a value of 4.1×10^{-18} M^2 reported for a similar dimeric GCN4 derivative bound to the CRE site (*10*).

Monomer Pathway. To study monomer binding (step 3) in isolation from dimer formation and dimer binding, we have designed the derivative C62GCN4$_{SS}^{one-leg}$. It contains the same leucine zipper domain as C62GCN4 but only a single DNA binding sequence. Because no two molecules of C62GCN4$_{SS}^{one-leg}$ can bind in the proper orientation to the CRE target site (*7*, *18*), the reaction with C62GCN4$_{SS}^{one-leg}$ conforms to step 3 alone. But even the binding of the basic region peptide BR conforms to step 3 alone, as demonstrated by isothermal titration calorimetry (Figure 5). Why no two molecules of BR can bind at the same time is not entirely clear. Since only part of BR is contacting the DNA (italicized residues in Table 1), the remaining residues of two bound molecules of BR may sterically interfere with each other unless kept properly oriented by the leucine zipper domain.

The association rate of the monomer is virtually the same as that of the dimer, 5×10^8 M^{-1} s^{-1}. The dissociation constant K_3 of step 3 is ~2 orders of magnitude larger than the K_2 of dimer binding because the complex MN dissociates faster, k_{-3} being around 50 s^{-1}. The complex with C62GCN4$^{one-leg}$ is more stable than that with BR, yet still 100 times less stable than the complex with dimeric GCN4. Kim and Little reported a K_2 of 1 μM for a complex corresponding to MN (*8*).

Step 4 of the monomer pathway could not be analyzed in a direct way. The equilibrium constant K_4 follows from the thermodynamic cycle and is 6×10^{-11} M for C62GCN4. Since the constants for the associations of monomeric and dimeric GCN4 are both $\sim 5 \times 10^8$ M^{-1} s^{-1}, it is reasonable to assume that binding of the second monomer in step 4 has a similar rate. With a k_4 of 5×10^8 M^{-1} s^{-1}, k_{-4} becomes 0.03 s^{-1}, at least 1000 times slower than the dissociation of the first monomer from the complex MN. This testifies to the high cooperativity between tethered ligands interacting with two adjacent binding sites (*39*). The degree of cooperativity can be quantified as K_3/K_4 or $(K_3)^2/(K_1K_2)$ (*8*). One obtains a value of 1600, which means that the probability of the second monomer staying on the DNA is 1600 times higher because it can dimerize with the first monomer through the leucine zipper domain.

Displacement of DNA from the Dimer−DNA Complex Is Very Slow. The rate of DNA displacement (Figure 6 and eq 9) should mirror the rate-limiting step of the dissociation of DN, which probably is the DN → DN* reaction step governed by k'_{-2}. Here, we note a discrepancy between the rate of DNA displacement and the kinetic constants for step 2. If one assumes $k'_{-2} = k_{disp} = 2.4 \times 10^{-4}$ s^{-1}, K_2 of C62GCN4 would be 3 pM,[2] 3 orders of magnitude less than K_2 from fluorescence titration. The K_2 of several bZIP transcription factor−DNA complexes is on the order of 1−10 nM, far from the picomolar range (*10*, *15*, *34*, *40*, *41*). Thus, it seems that displacement of DNA from the dimer−DNA complex does not monitor the overall dissociation rate of the complex and tends to overestimate its stability. In the presence of excess DNA during the exchange reaction, dimeric GCN4 may transiently bind to two molecules of double-stranded oligonucleotide, thereby slowing DNA exchange.

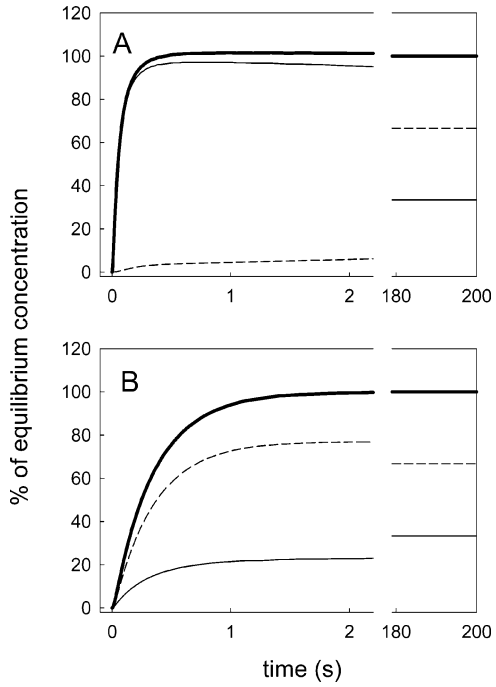

FIGURE 7: Comparison of the monomer and dimer pathways. The time course of formation of the complex DN via the monomer pathway (thin lines), the dimer pathway (dashed lines), and their sum (thick lines) are shown. (A) Forced monomer pathway. If the reaction starts from 100 nM monomer and 5 nM double-stranded DNA, more than 90% of the equilibrium concentration of the complex DN forms via the monomer pathway in less than 1 s. Although the buildup of the complex via the dimer pathway is very slow, more complex forms through the dimer pathway if the system is let to equilibrate because $k_{-1} \ll k_{-3}$. (B) *In vivo*-like situation. Letting the monomer and dimer pre-equilibrate (step 1) *before* addition of the DNA accelerates the dimer pathway. In the calculated example, 100 nM monomer was allowed to equilibrate to reach a $[M]_{equ}$ of 16 nM and a $[D]_{equ}$ of 42 nM before addition of 5 nM DNA. Calculations were performed by numerical integration using the following rate constants: $k_1 = 1.6 \times 10^7$ M^{-1} s^{-1}, $k_{-1} = 0.05$ s^{-1}, $k_2 = 3 \times 10^8$ M^{-1} s^{-1}, $k_{-2} = 30$ s^{-1}, $k'_{-2} = 10$ s^{-1}, $k'_{-2} = 0.1$ s^{-1}, $k_3 = 5 \times 10^8$ M^{-1} s^{-1}, $k_{-3} = 50$ s^{-1}, $k_4 = 5 \times 10^8$ M^{-1} s^{-1}, and $k_{-4} = 0.03$ s^{-1}.

Rates of DNA Binding through the Monomer and Dimer Pathway. We can now calculate the time course of complex formation through the monomer and dimer pathway using the experimentally determined rate constants of steps 1−3 together with the estimated rate constants of step 4. Figure 7 shows the results of a numerical integration of the four concerted reactions of Figure 1. In comparing the two pathways, one must distinguish between (i) starting the DNA binding reaction from free monomeric transcription factor alone and (ii) starting from pre-equilibrated monomeric and dimeric transcription factor in step 1. The latter condition may be closer to an *in vivo* situation in which monomeric and dimeric transcription factor compete for the DNA sites. If starting from monomeric transcription factor alone, DNA binding through the monomer pathway is very much faster than through the dimer pathway (Figure 7A). The reason is

[2] Calculated from the relationship $K_2 = (k_{-2}k'_{-2})/(k_2k'_{-2} + k_2k'_2)$.

the slower rate of monomer to dimer association in comparison to the rate of DNA binding of the monomer. However, if monomeric and dimeric transcription factor are at equilibrium before the reaction with the DNA, the dimer pathway is as rapid as the monomer pathway (Figure 7B). In the example of Figure 7B, more complex forms through the dimer pathway because [D] > [M] in pre-equilibrated step 1. It should be noted that the absolute rate of complex formation depends strongly on the initial concentrations of peptide and DNA and on the peptide/DNA ratio. For the calculation shown in Figure 7, we chose 100 nM monomer in 20-fold excess over the double-stranded DNA target. However, irrespective of the concentration and ratio of reactants, the general trend remains the same: DNA binding through the monomer pathway is more rapid if the reaction starts from monomeric transcription factor alone because dimer formation is relatively slow. However, the monomer and dimer pathways have similar rates if a substantial amount of dimer is present at the beginning of the reaction.

In their analysis of DNA binding of the Jun−Fos transcription factor based on fluorescence energy transfer between tagged Jun and Fos peptides, Kohler and Schepartz came to the conclusion that the dimer pathway is inadequate and unnecessary for complex formation (*15*). However, this conclusion holds only if all complex is formed from monomeric Jun, monomeric Fos, and DNA, which were the experimental conditions chosen by Kohler and Schepartz and in the calculations presented in Figure 7A. In a cellular environment, an equilibrium mixture of monomeric and dimeric transcription factors may be competing for DNA sites. If monomer and dimer bind at a similar rapid rate, as found here for GCN4, the choice of the pathway is influenced by the pre-existing ratio of monomeric to dimeric transcription factor. Hence, one would expect that a stable dimeric transcription factor could follow the dimer pathway under *in vivo* conditions.

We are well aware that the above conclusions are based on *in vitro* studies using a short target oligonucleotide and a truncated transcription factor. The assembly of a transcription factor−DNA complex *in vivo* is an intricate and complex affair. Not only must the transcription factor search its specific binding site in the presence of a large excess of unspecific DNA, but there also are other proteins competing for the DNA, much of it being packed in chromatin. Target finding occurs mainly by diffusion of the protein along the DNA (*42*−*44*). A monomeric transcription factor may diffuse more rapidly than a dimeric transcription factor because unspecific DNA binding of the monomer is weak. Unspecific DNA binding of the dimer could be stronger because of more nonspecific electrostatic interactions. Thus, the relative rates of diffusion of the monomer and dimer along the DNA are other variables affecting the time course of target recognition *in vivo*. Finally, accessory proteins influence the strength of the transcription factor−DNA complex (*45*). The rates of target finding and DNA binding through a monomer or dimer pathway could differ, depending on whether such accessory proteins bind to the monomeric or dimeric transcription factor, or both. In conclusion, there are many variables affecting the choice for a monomer or dimer recognition pathway *in vivo*. To clarify such complexity, future investigations must focus on the rates of diffusion of monomeric and dimeric transcription factors along the DNA and on the effect of other proteins on the stability of transcription factor−DNA complexes.

REFERENCES

1. Vinson, C. R., Sigler, P. B., and McKnight, S. L. (1989) *Science 246*, 911−916.
2. Baxevanis, A. D., and Vinson, C. R. (1993) *Curr. Opin. Genet. Dev. 3*, 278−285.
3. Hurst, H. C. (1996) *Leucine Zippers: Transcription factors*, 3rd ed., Academic Press, London.
4. Ellenberger, T. (1994) *Curr. Opin. Struct. Biol. 4*, 12−21.
5. Ellenberger, T. E., Brandl, C. J., Struhl, K., and Harrison, S. C. (1992) *Cell 71*, 1223−1237.
6. Glover, J. N. M., and Harrison, S. C. (1995) *Nature 373*, 257−261.
7. Keller, W., König, P., and Richmond, T. J. (1995) *J. Mol. Biol. 254*, 657−667.
8. Kim, B., and Little, J. W. (1992) *Science 255*, 203−206.
9. Park, C., Campbell, J. L., and Goddard, W. A. (1996) *J. Am. Chem. Soc. 118*, 4235−4239.
10. Metallo, S. J., and Schepartz, A. (1997) *Nat. Struct. Biol. 4*, 115−117.
11. Berger, C., Piubelli, L., Haditsch, U., and Bosshard, H. R. (1998) *FEBS Lett. 425*, 14−18.
12. Wu, X., Spiro, C., Owen, W. G., and McMurray, C. T. (1998) *J. Biol. Chem. 273*, 20820−20827.
13. Rentzeperis, D., Jonsson, T., and Sauer, R. T. (1999) *Nat. Struct. Biol. 6*, 569−573.
14. Kohler, J. J., Metallo, S. J., Schneider, T. L., and Schepartz, A. (1999) *Proc. Natl. Acad. Sci. U.S.A. 96*, 11735−11739.
15. Kohler, J. J., and Schepartz, A. (2001) *Biochemistry 40*, 130−142.
16. Vinson, C., Myakishev, M., Acharya, A., Mir, A. A., Moll, J. R., and Bonovich, M. (2002) *Mol. Cell. Biol. 22*, 6321−6335.
17. Bosshard, H. R., Dürr, E., Hitz, T., and Jelesarov, I. (2001) *Biochemistry 40*, 3544−3552.
18. König, P., and Richmond, T. J. (1993) *J. Mol. Biol. 233*, 139−154.
19. Berger, C., Jelesarov, I., and Bosshard, H. R. (1996) *Biochemistry 35*, 14984−14991.
20. Leder, L., Berger, C., Bornhauser, S., Wendt, H., Ackermann, F., Jelesarov, I., and Bosshard, H. R. (1995) *Biochemistry 34*, 16509−16518.
21. Kirsch, R. D., and Joly, E. (1998) *Nucleic Acids Res. 26*, 1848−1850.
22. Gill, S. C., and von Hippel, P. (1989) *Anal. Biochem. 182*, 319−326.
23. Brown, T., and Brown, D. J. S. (1991) in *Oligonucleotides and analogues: a practical approach* (Eckstein, F., Ed.) IRL Press, Oxford, U.K.
24. Bernasconi, C. F. (1976) *Relaxation kinetics*, 1st ed., Academic Press, New York.
25. Hinnebusch, A. G. (1984) *Proc. Natl. Acad. Sci. U.S.A. 81*, 6442−6446.
26. Hope, I. A., and Struhl, K. (1985) *Cell 43*, 177−188.
27. Landschulz, W. H., Johnson, P. F., and McKnight, S. L. (1988) *Science 240*, 1759−1764.
28. Hope, I. A., and Struhl, K. (1987) *EMBO J. 6*, 2781−2784.
29. Lee, W., Mitchell, P., and Tjian, R. (1987) *Cell 49*, 741−752.
30. Sellers, J. W., Vincent, A. C., and Struhl, K. (1990) *Mol. Cell. Biol. 10*, 5077−5086.
31. Kuzmic, P. (1996) *Anal. Biochem. 237*, 260−273.
32. Suckow, M., Schwamborn, K., Kisters-Woike, B., von Wilcken-Bergmann, B., and Muller-Hill, B. (1994) *Nucleic Acids Res. 22*, 4395−4404.
33. Zitzewitz, J. A., Bilsel, O., Luo, J. B., Jones, B. E., and Matthews, C. R. (1995) *Biochemistry 34*, 12812−12819.
34. Patel, L. R., Curran, T., and Kerppola, T. K. (1994) *Proc. Natl. Acad. Sci. U.S.A. 91*, 7360−7364.

35. von Smolukowski, M. (1917) *Z. Phys. Chem. 92*, 129−168.
36. Dürr, E., Jelesarov, I., and Bosshard, H. R. (1999) *Biochemistry 38*, 870−880.
37. Kozlov, A. G., and Lohman, T. M. (2002) *Biochemistry 41*, 6032−6044.
38. Ferreiro, D. U., and de Prat-Gay, G. (2003) *J. Mol. Biol. 331*, 89−99.
39. Kramer, R. H., and Karpen, J. W. (1998) *Nature 395*, 710−713.
40. Iakoucheva, L. M., Walker, R. K., van Houten, B., and Ackerman, E. J. (2002) *Biochemistry 41*, 131−143.
41. Metallo, S. J., and Schepartz, A. (1994) *Chem. Biol. 1*, 143−151.
42. von Hippel, P. H., and Berg, O. G. (1989) *J. Biol. Chem. 264*, 675−678.
43. Shimamoto, N. (1999) *J. Biol. Chem. 274*, 15293−15296.
44. Stanford, N. P., Szczelkun, M. D., Marko, J. F., and Halford, S. E. (2001) *EMBO J. 19*, 6546−6557.
45. Schneider, T. L., and Schepartz, A. (2001) *Biochemistry 40*, 2835−2843.

BI0355793